Available online at www.sciencedirect.com

SCIENCE DIRECT®

Geoderma 129 (2005) 279–290

GEODERMA

www.elsevier.com/locate/geoderma

The relationship between fractal properties of solid matrix and pore space in porous media

Annette Dathe[a,*], Martin Thullner[b]

[a]*Soil and Water Research Group, Biological and Environmental Engineering, Cornell University, 122 Riley-Robb Hall, Ithaca, NY 14853-5701, USA*

[b]*Department of Earth Science-Geochemistry, Faculty of Geosciences, Utrecht University, P.O. Box 80021, 3508 TA Utrecht, The Netherlands*

Received 2 June 2004; received in revised form 6 December 2004; accepted 6 January 2005
Available online 11 March 2005

Abstract

Measuring fractal dimensions has become a common practice for describing structural properties of porous media. Depending on the object of interest, different features of the structure can be measured: solid matrix, pores, and the interface between them. However, when measuring the fractal dimension of all these features, the question arises whether these dimensions are independent from each other or whether they can be related to an underlying property of the structure or image, respectively.

For a variety of porous media we measured the fractal dimension of the matrix, the pore space, and the interface between them simultaneously using the box counting method. Analyzed images were obtained from soil thin sections and a void system in a clayey soil.

Measured fractal dimensions were compared with fractal dimensions estimated by the pore-solid fractal (PSF) model, which derives the fractal properties of the matrix and the pore space completely as a function of the porosity, the size of the initiator and the fractal dimension of the interface. Measured results agree well with values obtained from the PSF model. A clear relationship between the fractal dimensions of the two phases (solid matrix and pore space) of a porous medium and their interface was observed. For all images the smallest fractal dimension was found for the interface between matrix and pores. Values for the fractal dimension of the two phases were between those for the interface and the Euclidian space with the phase with the lower mass fraction always having the smaller dimension. Porosity was found to act as weighing factor linking the dimension of the phases to those of the interface and Euclidian space. Model results also predict a dependency of the dimension of the phases on the spatial resolution of the analyzed image. For images having a high resolution (compared to the size of the initiator) phase dimensions are expected to be greater than for images having a low resolution.

Keywords: Soil structure; Fractal dimension; Porosity; Interface; Image analysis

* Corresponding author. Tel.: +1 607 255 2049; fax: +1 607 255 4080.
E-mail address: ad273@cornell.edu (A. Dathe).

0016-7061/$ - see front matter © 2005 Elsevier B.V. All rights reserved.
doi:10.1016/j.geoderma.2005.01.003

1. Introduction

Deriving the physical properties of a porous medium (e.g., hydraulic conductivity, thermal conductivity, water retention curve) from parameters describing the structure of the medium (e.g., porosity, pore size distribution, specific surface area) is an ongoing challenge for scientists. As natural porous media commonly have a highly complex structure, such calculations cannot usually be done directly. A more common approach is to generate artificial structures, which allow calculating their physical properties. To allow such calculations these artificial structures have to be simplifications of the natural media they aim to represent. However, in order to yield representative results, the key structural properties of a natural porous medium have to be reproduced by the artificial structure. Therefore, the question arises how to generate an artificial porous medium fulfilling both of the above requirements. Soils are among the most prominent examples of naturally occurring porous media. Thus, in this study we will focus on soil structures as typical representatives of porous media.

A variety of approaches have been introduced to generate artificial porous structures. These approaches include the generation of regular pore networks (e.g., Berkowitz and Ewing, 1998), networks developed according to morphologically determined parameters of a soil (Vogel, 2000), the simulation of sedimentation processes (Dutta and Tarafdar, 2003), and the use of fractal models. For the latter, a minimum requirement for the applicability of the model is that the natural porous medium exhibits a self-similar scaling, described by its fractal dimension. This implies that the fractal properties measured for a natural porous medium can be appropriately reproduced by the fractal model.

To verify the assumption of a porous medium having a self-similar scaling behavior, fractal dimensions of various features have been determined experimentally. Measured features include particle size (measured with classical soil physics methods like sieving or sedimentation), size of soil aggregates (Turcotte, 1986; Young and Crawford, 1991; Perfect et al., 1993), and pore size, the latter derived from water retention curves (Ahl and Niemeyer, 1989; Perfect et al., 1996; Niemeyer and Machulla, 1999) or mercury intrusion curves (Bartoli et al., 1991; Bartoli et al., 1999). The inner surface of a porous medium is commonly determined from digital images of soil thin sections or soil blocks (Anderson et al., 1996; Bird et al., 1996; Pachepsky et al., 1996; Gimenez et al., 1997; Bartoli et al., 1999; Dathe et al., 2001).

In this study we use image analysis to quantify the self-similarity or the fractal dimension of the structure, respectively. Image analysis is a method for directly obtaining the structure of a porous medium, which is beyond a simple observation. In previous work, Dathe et al. (2001) measured the fractal dimension of the interface between soil particles and the pore space. They used images obtained from thin sections with a SEM (scanning electron microscope) using different magnifications or resolutions, respectively. Other authors investigated distinct features. Bartoli et al. (1991) measured the fractal dimension of soil matrix and pore space. To obtain images, they placed thin sections as negatives in a photograph chamber and used SEM and TEM (transmission electron microscopy) for high resolutions. Using black and white photographs from soil thin sections, Anderson et al. (1996, 2000) measured the mass dimension of the solid and the pore phase, respectively, and in addition the spectral dimension. Gimenez et al. (1998) measured the mass fractal dimension of the pore phase and the fractal dimension of the pore surface. Their images were obtained with a lens from polished blocks.

The question arises regarding which feature (e.g., grain or pore size distribution, mass of the pore phase, mass of the solid matrix phase, interface between pores and matrix) can be considered as representative for the porous medium as a whole. This also includes the question whether measuring the fractal dimension of one feature is sufficient for describing the fractal behavior of the entire structure.

Besides the challenge of evaluating the fractal properties of a porous medium experimentally, predictions of the fractal model also depend on the specific modeling approach. Most of the fractal models used describe a porous medium as a set of one fractal phase (matrix or pore) and its complementary non-fractal phase. In an iterative process, the fractal phase of an initial structure (initiator) is refined using a deterministic or stochastic pattern. This approach is described by the size of the initiator, the

ratio between both phases in the initiator, and a scaling rule, which describes the number of subpatterns into which the initial structure is divided. Being the basic model for this process, the well-known Sierpinski carpet (in two dimensions) or Menger sponge (in three dimensions) have commonly been used in several variations (Tyler and Wheatcraft, 1990; Rieu and Sposito, 1991; Crawford et al., 1993; Perrier et al., 1999; Rappoldt and Crawford, 1999; Lehmann et al., 2003). Other authors (Sukop et al., 2001) used alternative algorithms to create fractal porous media.

The drawback of these approaches is that the mass of the fractal phase (i.e., the phase, which is divided into smaller and smaller objects) approaches zero in case of an infinite number of iterations (Crawford et al., 1993; Crawford and Matsui, 1996; Perrier et al., 1999; Anderson et al., 2000). Therefore, most of these models deal with prefractals, wherein the iteration process is stopped at a point where the size of the smallest pores or grains is assumed to be reached. To overcome this problem, Perrier et al. (1999) introduced a generalized 'pore-solid fractal' (PSF) model, which assumes a generated porous medium to contain a third undefined phase in addition to the pore and the solid matrix phase. The iterative refinement process affects only this undefined phase, whereas the pore and matrix phases, once defined, are not subject to any further refinement. A relation can be derived from the PSF model between the scaling behavior of the mass of the pores, the mass of the solid matrix, and the interface between them.

An explicit comparison between the model predictions and measurements of the fractal geometry of natural porous media has not been done so far. Thus, the aim of the present study is to prove whether the dimensions of natural porous media can be described with the PSF model. Furthermore, we want to investigate whether the fractal dimensions of solid mass and pore space are explicitly related. To do so, fractal dimensions of the pore phase, the matrix phase, and the interface between them are measured simultaneously by image analysis. Measured results are compared with predictions of the PSF model to evaluate its applicability and to establish a general relation between the different parameters describing the fractal properties of porous media.

2. Materials and methods

2.1. Samples and sample preparation

Images of two different soil structures were chosen for investigation. One of the soil structures (Luvisol developed on Loess, county of Göttingen, Germany) was analyzed on the pore scale. Images for three different magnifications or resolutions, respectively, were obtained on the μm scale from polished surfaces of soil thin sections using a field emission SEM (Fig. 1a–c). The signal used for detection was composed of 3/4 backscattered and 1/4 secondary electrons at an electron acceleration energy of 18 keV, yielding a depth of focus of about 1 μm. Regions for the investigated images were selected arbitrary, from one thin section for image SEM 1, and from another thin section for images SEM 2 and 3. The thin sections were oriented horizontally in

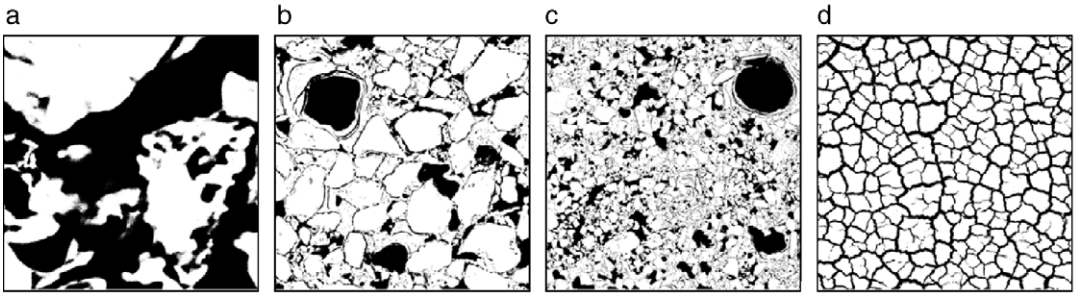

Fig. 1. Binary images as they have been used for the measurements of the fractal dimension. Objects are shown in white; pores or voids, respectively, in black. The images present a soil structure obtained from thin sections using SEM (a–c) and a soil void system (d). The original size of the images shown is (a) 30 μm, (b) 266 μm, (c) 890 μm, and (d) 560 mm.

relation to the block they had been cut off. Dathe et al. (2001) described in detail the procedure of preparing the samples and obtaining the images. The second soil structure (Pelosol containing about 80% clay, Darling Basin, Australia) represents a soil void system, which can be observed on a larger scale (~10 cm). Changing water content causes the swelling and shrinking of the clay minerals, yielding the development of voids (Fig. 1d).

SEM images were obtained as grey scale images, and Fig. 1d shows a digital scan of a top view photo of the soil surface taken by an analog camera. All images were stored with 1024^2 pixel resolution, whereas their original size increases from a side length of 30 μm to 560 mm (Table 1).

2.1.1. Image analysis

Image analysis was performed using a Zeiss KS400 system (Zeiss Vision, Jena, Germany) applying user-defined macros (Eins, 1998). In order to obtain a binary image, the original image had to be thresholded. Whereas the SEM images were obtained as 8-bit images (256 grey values for each pixel), the scan of the photo of the soil void system was obtained as 24-bit image, i.e., 8 bits for every color channel. For the SEM images, we took advantage of the clear contrast between the dark pores and the bright matrix, assuming a normal distribution of the related grey values for the pores and the matrix, respectively. The scan of the soil void system showed two maxima for the grey values obtained as the average of the three-color channels. The image was segmented at the minimum of the grey value distribution between the maxima for the voids and the matrix.

2.1.2. Measurement of fractal dimensions

We used the box counting method to measure fractal dimensions, or more specifically, fractal capacity dimensions of the pore and the matrix phase. These dimensions can be described by the ratio between the logarithm of an iteration rule and the logarithm of the scale increment (Mandelbrot, 1983).

Table 1
Comparison between calculated and measured fractal dimensions for the measured and the corrected (marked with ‡) porosity

Image	Resolution (∝m/pixel)	Range box size (pixel)	Measurement				Model Results			
			Model Input				Method (A)		Method (B)	
			D_p	D_m	Porosity	D	D_p	D_m	D_p	D_m
SEM 1	0.03	2 - 128	1.863 (0.007)	1.845 (0.010)	0.513	1.368 (0.042)	1.859 (0.017)	1.848 (0.018)	1.851 (0.011)	1.840 (0.012)
SEM 2	0.26	2 - 64	1.638 (0.022)	1.947 (0.003)	0.230	1.387 (0.079)	1.673 (0.023)	1.936 (0.009)	1.674 (0.022)	1.932 (0.006)
					0.249‡		1.688‡ (0.023)	1.930‡ (0.009)	1.688‡ (0.020)	1.925‡ (0.005)
SEM 3	0.87	2 - 64	1.707 (0.058)	1.943 (0.007)	0.264	1.526 (0.110)	1.740 (0.014)	1.932 (0.007)	1.741 (0.031)	1.929 (0.010)
					0.307‡		1.764‡ (0.014)	1.919‡ (0.008)	1.764‡ (0.028)	1.916‡ (0.011)
Voids	547.30	2 - 32	1.530 (0.017)	1.921 (0.017)	0.227	1.112 (0.129)	1.557 (0.044)	1.918 (0.015)	1.557 (0.030)	1.909 (0.005)
					0.238‡		1.570‡ (0.044)	1.914‡ (0.016)	1.569‡ (0.030)	1.904‡ (0.006)

The model input parameter for the initiator equals the upper range of box sizes. Values for the errors are given in brackets and explained in the text.

The measurement method takes advantage of the assumed self-similar scaling behavior, which allows applying the equation

$$N(r) \propto r^{-D}. \quad (1)$$

The power law describes the number of boxes N of a specific feature as a function of their side length r with an exponent D. Thus, whenever measured box counts can be described by Eq. (1) using a non-integer value for D, the feature is considered to be a fractal with D as the fractal dimension (see, e.g., Baveye and Boast, 1998 for a review on the general validity of this assumption).

Measurements were performed starting with a box size of two pixel, and increasing the box size by powers of 2, until the size of the image was reached at 2^{10}=1024. This was done separately for the matrix as well as for the pore space or background, respectively. For the estimation of the fractal dimension, the data were used up to the box size where no further structure information could be obtained. I.e., the generator L of the fractal set (see below) was set to the maximum box size, for which the boxes covering a specific feature did not cover the entire image. The fractal dimension was estimated separately for the matrix and the pore space as the slope of a log–log plot according to

$$\log N(r) = -D\log r + c. \quad (2)$$

For estimating the fractal dimension of the pore–matrix interface, the number of boxes covering the interface (N_s) was taken as the number of boxes covering pores and matrix (N_p and N_m) simultaneously as

$$N_s(r) = N_m(r) + N_p(r) - N_{max}(r) \quad (3)$$

with N_{max} as the total number of boxes needed to cover the entire image.

2.2. Model description

The model used within this study is the 'pore-solid fractal' (PSF) model as introduced by Perrier et al. (1999). To our knowledge, this is the only fractal model approach which preserves a finite volume for both phases of a soil structure. The general approach of the PSF model is dividing a given region with linear size L into subsections with the linear size L/n. A generator assigns one of the following phases to each subsection: pore phase, matrix phase, or a third undefined phase, with each phase having a predefined proportion of the entire region. In a subsequent step, the third undefined phase of the initiator is again divided into the three different phases using the same proportions. In contrast, the pore and the matrix phase are kept as determined by the previous steps. An iterative repetition of these steps then creates a structure with pores and matrix solids of various sizes (Fig. 2).

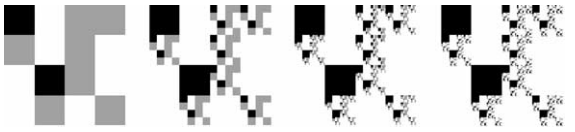

Fig. 2. Concept of the pore-solid fractal model for the first three iterations. The initiator is divided into matrix (white), pores (black) and an undefined set shown in grey. For each iteration step only the grey subregions are replaced by the initiator. Modified from Perrier et al. (1999).

For an infinite number of iterations, the mass of the undefined phase approaches 0, but the mass of the pores and the mass of the matrix each maintain a finite value. The porosity ϕ of the structure finally approaches $\phi = x/(x+y)$, with x and y as the fraction of the pore phase and the matrix phase, respectively, within the initial generator (Perrier et al., 1999). The fact that for the PSF model, pore phase and matrix phase have a finite (non-zero) mass even for an infinite number of iterations marks an important difference from fractal pore models assuming two phases only. For the latter models, one phase – either the pore phase (pore mass fractal) or the solid matrix (solid mass fractal) – disappears in the case of an infinite number of iterations, with the mass of this phase thus approaching 0. As a consequence, the number of iterations has to be limited for creating a porous structure containing pores and a solid matrix. Therefore, the properties of the resulting structure are functions of the number of iterations.

For the PSF model the fractal dimension D of the porous medium is given by

$$D = d + \frac{\log(1 - x - y)}{\log n} \quad (4)$$

with d as the Euclidian dimension of the structure. The proportions of the pore phase and the matrix phase within the generator are given by x and y, respectively. Note that the proportion z of the undefined phase is given by $z=1-x-y$.

When calculating the fractal properties of the pore mass, the solid matrix mass, and the interface between them, it has been shown that only the interface exhibits fractal scaling with the fractal dimension D, whereas the pore mass and the solid mass do not scale with a fractal dimension (Perrier et al., 1999). However, the PSF model allows calculation of the results of analyzing the mass of the pores and the solid matrix by the box counting method as:

$$N_p(r) = \frac{x}{x+y} L^d r^{-d} + \frac{y}{x+y} L^D r^{-D} \tag{5a}$$

$$N_m(r) = \frac{y}{x+y} L^d r^{-d} + \frac{x}{x+y} L^D r^{-D} \tag{5b}$$

with N_p and N_m as the number of box counts using boxes with linear size r. Using $x/(x+y)=\phi$ and $y/(x+y)=(1-\phi)$ reduces the number of parameters determining the box counts to four: the Euclidian dimension d, the fractal dimension D of the porous medium, the porosity ϕ, and the size of the initiator L.

To compare the results of the PSF model with measured results for natural porous media analyzed by digital image analysis, Eqs. (5a) and (5b) were used with parameter values taken from the image analysis procedure. Here we assumed that according to the PSF model the fractal dimension D is given by the fractal dimension measured for the interface between pore phase and matrix phase for each analyzed porous medium. Porosities ϕ were calculated using the distribution of black and white pixels in the binary version of the digital images. It was assumed that the ratio ϕ^* between the black pixels (representing the pore space) and the total pixels (black and white) is underestimating the porosity of porous media with small porosities. This is caused by the binarization process, which is using the grey scale of each pixel to determine the binary value. Thus, porous structures smaller than the size of a pixel are converted into either pore space or matrix. Assuming a fractal scaling of the porous medium, the mass fraction of these subpixel scale structures is given by the porosity of the entire medium. As a consequence, the grey scale of these pixels is dominated by the phase with the greater mass fraction. I.e., for media having a small porosity all these "grey" pixels converted into white pixels, causing the underestimation of the porosity. To compensate this effect and to get an estimate of the real porosity of the porous medium, the PSF model was used to calculate the correction term. Considering a porous structure following the PSF model the number of black, white and grey pixels (N_b, N_w, and N_g) can be calculated using Eqs. (6a)–(6c) for a box size of 1 pixel:

$$N_b = N_p(r=1) - N_s(r=1) \tag{6a}$$

$$N_w = N_m(r=1) - N_s(r=1) \tag{6b}$$

$$N_g = N_s(r=1). \tag{6c}$$

When assuming a small porosity, the binarization process is transferring all grey pixels into white pixels and, thus, the number of black pixels in the binary image (N_b^*) is:

$$\begin{aligned} N_b^* = N_b &= N_p - \left(N_p + N_m - L^d r^{-d}\right) \\ &= L^d r^{-d} - \left(\frac{y}{x+y} L^d r^{-d} + \frac{x}{x+y} L^D r^{-D}\right) \\ &= \phi\left(L^d r^{-d} - L^D r^{-D}\right) \end{aligned}$$

Therefore, the real porosity ϕ is linked to the measured porosity $\phi^*=N_b^*/(L^d r^{-d})$ by

$$\phi = \frac{\phi^*}{1 - L^{(D-d)} r^{-(D-d)}}. \tag{7}$$

The size L of the initiator was determined by the largest box size, which allowed resolving any properties of the imaged structure (i.e., the number of box counts for a specific phase is not covering the entire image). For the digital images analyzed within this study values for ϕ^* vary between 0.227 and 0.513. We assumed that for the image SEM 1 the measured porosity of 0.513 is great enough not to be affected significantly by the binarization process. For the other three images having measured porosities

between 0.227 and 0.264 we used Eq. (7) to estimate the real porosity.

Thus, for an image of linear size N, the number of box counts according to the PSF model is given by

$$N_{\mathrm{p}}(r) = \left(\frac{N}{L}\right)^{d}\left(\phi L^{d} r^{-d} + (1-\phi)L^{D} r^{-D}\right) \tag{8a}$$

$$N_{\mathrm{m}}(r) = \left(\frac{N}{L}\right)^{d}\left((1-\phi)L^{d} r^{-d} + \phi L^{D} r^{-D}\right). \tag{8b}$$

Using Eqs. (8a) and (8b) box counts were calculated for the box sizes used for the image analysis. The fractal dimension of the porous structure was assumed to be given by the dimension of the interface between pores and matrix, and values measured by image analysis were taken as input for the model.

Model results were analyzed using two different methods:

(A) Analogous to the image analysis method, results were plotted on a log–log scale and fitted by a power law to obtain the "fractal" dimension for the mass of the pore phase and the solid matrix phase, respectively.

(B) "Fractal" dimensions D were calculated by determining the derivatives of Eqs. (8a) and (8b) on a log–log scale using $x=L/r$:

$$D_{\mathrm{p}}(x) = \frac{\partial \ln N_{\mathrm{p}}}{\partial \ln x} = D + (d-D)\frac{\phi}{\phi + (1-\phi)x^{(D-d)}} \tag{9a}$$

$$D_{\mathrm{m}}(x) = \frac{\partial \ln N_{\mathrm{m}}}{\partial \ln x} = D + (d-D)\frac{1-\phi}{(1-\phi) + \phi x^{(D-d)}}. \tag{9b}$$

Only if pore and matrix phase are fractals, D_{p} and D_{m} would not depend on x. Thus, performing method (B), an average D was calculated to compare the model derived D-values with those from the measurements. As the box sizes used for the measurements were equally distributed on the log scale, we calculated for each image the arithmetic mean of $D(x)$ with x-values given by the initiator sizes

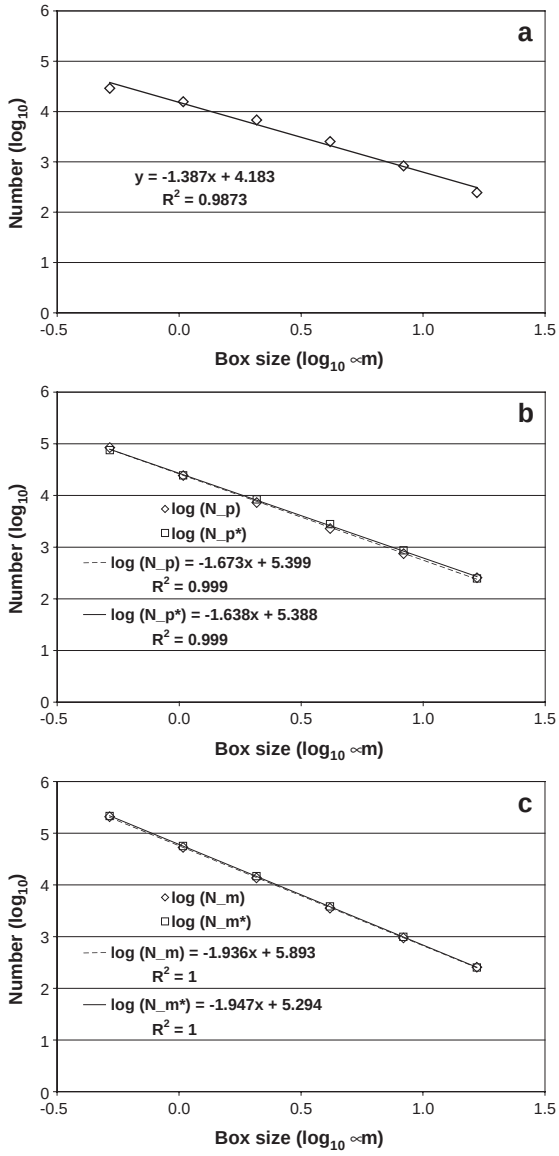

Fig. 3. Box counts as measured with image analysis and estimated according to the pore-solid fractal model for image SEM 2. The slope of the linear regression yields the fractal dimensions using measured box counts and box counts estimated from the model with method (A). Shown are (a) number of boxes for the interface as determined from the measured counts using Eq. (3), (b) estimated (N_p) and measured (N_p*) number of boxes for the pore space and (c) estimated (N_m) and measured (N_m*) number of boxes for the matrix space.

determined for each image and the box sizes used for the measurements.

3. Results

3.1. Image analysis

Measured box counts for the interface calculated using Eq. (3) as well as box counts for the pore and the matrix phase are shown for image SEM 2 as an example (Fig. 3). According to Eq. (2), for all images the fractal dimensions were obtained as the slope of the log–log plot of measured box counts as a function of box size. Measured fractal dimensions D varied between 1.112 for the interface of the soil void system to 1.947 for the solid mass of the image SEM 2 (Table 1). For all images, the interface had the smallest dimension, followed by the dimension of the pore phase, with the dimension of the matrix phase having the highest value. An exception was image SEM 1, for which the dimension of the pore phase was greater than the dimension of the matrix phase. For this image the pore phase had a greater mass than the matrix phase, i.e., the porosity was greater than 0.5. Thus, for all images the phase with the greater mass also had a greater fractal dimension than its corresponding phase. Measured fractal dimensions of the pore–matrix interfaces for images SEM 1, SEM 2, and SEM 3 yield D=1.368, D=1.387, and D=1.526, which are greater than the interface dimension for image Voids (D=1.112). Values for the measured porosity ranged from 0.227% for the image Voids to 0.513 for SEM 1. For small porosities, the differences between fractal dimensions of pore and matrix phase were larger than for porosities close to 0.5. As a measurement for the goodness of fit, the standard error of the slope, which is the standard error of each linear regression divided by the square root of the sum of squares of box sizes used, is given for all images. Values for this analysis are taken as logarithms, and the procedure does not take into account that for each image data obtained for a given box size are not independent from those obtained for other box sizes. Considering these dependencies would lead to enlarged standard errors (Reeve, 1992). Standard errors for the phase with the greater mass were lower than for the complementary phase of the same image. Standard errors of the fractal dimension of the interface were greater than those of the pore phase and the matrix phase, respectively.

3.2. PSF model

As for the measured values, box counts calculated according to the PSF model using method (A) are shown for SEM 2 as an example (Fig. 3b and c). Values for the model parameters obtained from the measurements are shown in Table 1 as well as the fractal dimensions estimated with the PSF model. As described above, results for method (A) were determined by fitting the box counts calculated using Eqs. (8a) and (8b), and for method (B) results were calculated using Eqs. (9a) and (9b). The size of the initiator L used in the PSF model is given by the maximum of the box size range for each image. The results of the two methods were nearly identical for all images, with greatest differences (D_m of image Voids) being within the given error range. For each image the model-based dimensions showed the same sequence as observed for the measurement: the phase with the smaller mass had a smaller dimension than its complementary phase. Naturally, the dimensions of both phases were larger than the dimension of the interface and smaller than the Euclidian dimension of the structure.

3.3. Comparison of results

Comparing the model results with the results from image analysis showed generally a good agreement between model derived dimensions and measured dimensions of the pore and matrix phase. For D_p, differences between results from image analysis and from the model did not exceed 0.057, whereas for D_m these differences were smaller than 0.027 (see results for SEM 3, Table 1). For SEM 1, the results of method (A) were closer to the measured results. For SEM 2, SEM 3, and the Voids image, results obtained with porosities corrected using Eq. (7) showed a worse agreement with the measurements than the results obtained with the measured porosities. For most cases, model results tended slightly to overestimate the dimension of the smaller phase, whereas the dimension of the larger phase was underestimated by the model. An exception was

method (B) for SEM 1, where the dimension of the smaller phase was underestimated. Taking the standard error of the slope as a measurement for the goodness of fit, the fractal dimensions measured with image analysis were more accurate than the fractal dimensions determined according method (A). The only exception was the matrix of the Voids image: for this image the accuracy of the model fit exceeded the measurement. Error values given for method (B) are estimated from the errors of each $D_{p,m}(x)$ as caused by measurement errors for D and ϕ (for ϕ errors we used the difference between ϕ and ϕ*if available; otherwise we assumed an error of 10%). As the error ranges were determined differently, a comparison of errors between measurement and method (A), and method (B) is difficult. Nevertheless, error ranges are similar for both methods and for the measurement, with errors always being greater for the dimension of the phase with the lower mass fraction.

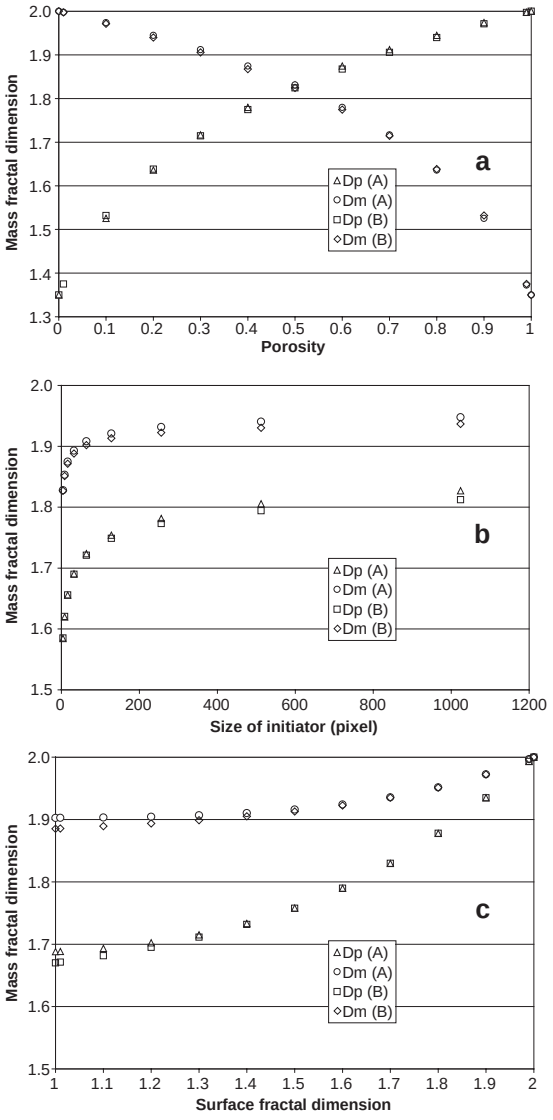

Fig. 4. Sensitivity of model results using methods (A) and (B). Shown are D_p and D_m for (a) increasing porosities ϕ, (b) increasing size of the initiator L, and (c) increasing surface fractal dimension D. When fixed, values are set to ϕ=0.31, L=64, D=1.35, which are approximately the means of the measured values shown in Table 1.

3.4. Sensitivity of model results

To investigate the model parameters' influence on the mass fractal dimension of the pore and the matrix phase (D_p and D_m), a sensitivity analysis was performed for the porosity ϕ, the size of the initiator L, and the surface fractal dimension D. An artificial structure (size 1024^2) was analyzed with values of ϕ=0.31, L=64, and D=1.35 using mean values from Table 1. Results of this analysis which was performed for both methods, (A) and (B), show that the sensitivity of D_p and D_m is highest towards variations of porosity (see Fig. 4a). The porosity determines the difference between D_p and D_m. For a porosity of ϕ=0.5 the dimensions are equal, and for ϕ>0.5 results are symmetrical to those for inverted phases and porosity $1-\phi$. For $\phi\rightarrow 0$ or $\phi\rightarrow 1$, respectively, the dimension of the disappearing feature approaches the dimension of the interface. Variations of the size of the initiator L also have a high influence on D_p and D_m, especially for relatively small L which includes the sizes we obtained (see Table 1 and Fig. 4b). Generally, the dimension of the phase with the larger mass shows a smaller sensitivity towards changes of ϕ and L. An increase of D yields higher values for D_p and D_m until they reach the Euclidian dimension of 2, whereas their difference decreases for greater D (Fig. 4c). Differences between method (A) and (B) are most pronounced for large sizes of the initiator and small surface fractal dimensions.

4. Discussion

4.1. Experimental observations

For all features (pore phase, matrix phase, pore–matrix interface) of the investigated images, the measured box counts could be successfully fitted by a power law with a noninteger exponent. This indicates a fractal scaling behavior of each measured feature. However, a comparison of the fractal dimensions measured for the different features of a porous structure demonstrates that the scaling behavior of each feature was different. This experimental finding is in agreement with the work of other authors (Crawford and Matsui, 1996; Anderson et al., 2000) who measured greater fractal dimensions for the solid phase than for the pore phase. Thus, measuring the dimension of an arbitrarily chosen feature does not provide sufficient information on the fractal properties of a structure. For each image the measured dimensions had the same sequence (interface < smaller phase < larger phase < Euclidian space), which suggest the existence of a relation between the dimension of the different features, although no obvious relation can be extracted from the measurement itself.

4.2. Model applicability

To establish a relation between the fractal dimensions of different features of a porous medium and to evaluate the applicability of the PSF model, measured data were compared to model results showing that the findings of the measurements could be reproduced by the model. For all images the model-based fractal dimensions were in good agreement with the measured dimensions (see Fig. 3b and c for an example). The model was reproducing the measured sequence of the fractal dimensions, and differences between the values of each measured and model based fractal dimension were within or at least close to the standard errors. The fact that the differences between results of the two methods used to analyze the model were relatively small suggests that the model was indeed reproducing the fractal properties of the investigated porous structure and that the good agreement between the model and the measurements was not biased by an arbitrarily chosen analysis method. The good agreement between model and measurement was not granted a priori, as the model considers the pore and the matrix phase not to be fractals. However, analyzing the box counts calculated from the model indicated that those box counts could be nicely fitted by a power law, with errors only slightly larger than those obtained when fitting the measured box counts. Hence, using the same criteria as applied to the measured box counts would justify the use of the term “fractal” when describing these features. Within the accuracy of the measurements presented here it was not possible to distinguish between the phases being fractals or having a mixed, fractal and Euclidian, behavior as predicted by the model. In contrast, the model assumed the interface being a fractal. This would suggest that the box counts for the interface were exactly determined by a power law. Thus, the fact that the measured box counts for the interface suggest a slightly nonlinear dependency on the box size (on a log–log scale, see Fig. 3a) and that for all images errors for fitting the box counts for the interface were larger than the errors obtained for the two phases indicates a discrepancy between model assumptions and measured properties of the porous structures. From the PSF model one would also expect the same values for the fractal dimension of the interface, and the porosity for all three SEM images, as they were obtained from the same soil structure. The apparently observed differences between these values may be attributed to the heterogeneity of the soil structure (not being a mathematically generated fractal but exhibiting fractal behavior in a statistical manner only), but may also indicate a discrepancy between the PSF model and natural porous media. Another reason might be the surface of the single grains being very smooth, thus, determining a lower limit for self-similarity of the investigated structure (Dathe et al., 2001).

4.3. Influence of porosity on fractal properties of porous media

The good agreement between measured and model based fractal dimensions suggests that the model defines a structure equivalent to the porous structures investigated here. In the model, the box counts or

fractal dimensions, respectively, were composed by two components: an Euclidian term, and a fractal term given by the fractal dimension of the interface (see Eqs. (8a), (8b), (9a) and (9b)). For the pore phase the Euclidian component is weighted by ϕ, and the fractal component is weighted by $(1-\phi)$. For the matrix phase the weighting factors are exchanged. This led directly to the observed sequence for the fractal dimensions with both phase dimensions being between the dimension of the interface and the Euclidian dimension and the smaller phase having the smaller dimension. This porosity dependence also indicates that the asymptotic behavior for $\phi \rightarrow 0$ or $\phi \rightarrow 1$ is different for the two phases. The closer the smaller phase gets to a fractal the less this assumption holds for the larger phase. They cannot be assumed to be fractals simultaneously, which again indicates that measuring the fractal properties of one phase only does not allow to make any predictions on its complementary phase.

4.4. Importance of measurement process

Besides the porosity, model predictions for the phase dimensions also depend on the size of the initiator L, as well as on the box sizes used for the image analysis r, or on their combination, the variable $x=L/r$, respectively. Theoretically, x-values range from 1 to ∞. Using Eqs. (9a) and (9b) this determines the range of possible values for D_p and D_m to: $D(1-\phi)+d\phi<D_p<d$ and $d(1-\phi)+D\phi<D_m<d$. This is in accordance to theoretical considerations for the PSF model (Bird and Perrier, 2003). For comparing model predictions obtained for method (B) with measured results it was necessary to calculate the average dimension, which is representative for the x range corresponding to the measurements, and thus, the resulting dimension strongly depends on the resolution of the measuring procedure. For a given resolution, results depend on the size of the initiator and the sensitivity is highest for small values of L including the range of values observed within this study. This also indicates that the uncertainty associated with the determination of the initiator size has a high impact on the outcome of the model. We decided to determine the initiator size from the measured box counts, trying to apply a consistent procedure to all images. The uncertainty of this procedure is given by the factor of 2 between two consecutive box sizes.

For a given initiator size the range of possible x-values depends on the image resolution. The finer the resolution the larger is the range of x-values (note that $x \propto (1/r)$). As $D_{p,m}(x)$ increases monotonically with x, a larger x range will lead to larger estimates for the dimension of the pore and matrix phase with both dimensions eventually approaching d. This would imply that the self-similarity of the porous structure can be extrapolated to smaller length scale ad infinum, which ignores that there is a limit for this self-similarity (see Section 4.2). In contrast to a high resolution, a coarse resolution of the analyzed image narrows the range of x-values, bringing the estimates for the pore phase and the matrix phase dimension closer to $D(1-\phi)+d\phi$ and $d(1-\phi)+D\phi$, respectively. A dependency of measured fractal dimensions on the observation scale has been reported in the literature (Dathe and Baveye, 2003), but the dependency of x on L and r complicates the comparison of the result of different studies.

5. Conclusions

Measuring fractal dimensions of a porous medium yields different results depending on the measured feature (pore phase, matrix phase, pore–matrix interface). These findings could be reproduced well by the PSF model suggesting that only the pore–matrix interface is a fractal, whereas the pore and the matrix phase are composed by a fractal component defined by the dimension of the interface and an Euclidian component. The porosity of a medium was found to be the weighting factor for these components. Although not being a fractal, pore and matrix phase can be well approximated by a power law with the "fractal" dimension being a function of the dimension of the interface, the porosity, the size of the initiator, and the spatial resolution of the measurement.

Acknowledgements

This study was in part funded by the German Science Foundation under grant number DA 575/1-1. Philippe Baveye, Laboratory of Geoenvironmental

Science and Engineering, Cornell University, is acknowledged for additional material support. The image analysis was carried out at the Cornell Institute for Resource Information Systems (IRIS). We like to thank Stephen DeGloria for providing this opportunity.

References

Ahl, C., Niemeyer, J., 1989. The fractal dimension of the pore-volume inside soils. Zeitschrift fur Pflanzenernahrung und Bodenkunde 152, 457–458.

Anderson, A.N., McBratney, A.B., FitzPatrick, E.A., 1996. Soil mass, surface, and spectral fractal dimensions estimated from thin section photographs. Soil Science Society of America Journal 60, 962–969.

Anderson, A.N., Crawford, J.W., McBratney, A.B., 2000. On diffusion in fractal soil structures. Soil Science Society of America Journal 64, 19–24.

Bartoli, F., Philippy, R., Doirisse, M., Niquet, S., Dubuit, M., 1991. Structure and self-similarity in silty and sandy soils—the fractal approach. Journal of Soil Science 42, 167–185.

Bartoli, F., Bird, N.R.A., Gomendy, V., Vivier, H., Niquet, S., 1999. The relation between silty soil structures and their mercury porosimetry curve counterparts: fractals and percolation. European Journal of Soil Science 50, 9–22.

Baveye, P., Boast, C.W., 1998. Fractal geometry, fragmentation processes and the physics of scale invariance: an introduction. In: Baveye, P., Parlange, J.Y., Stewart, B.A. (Eds.), Fractals in Soil Science. CRC Press, Boca Raton, pp. 1–54.

Berkowitz, B., Ewing, R.P., 1998. Percolation theory and network modeling applications in soil physics. Surveys in Geophysics 19 (1), 23–72.

Bird, N.R.A., Perrier, E.M.A., 2003. The pore-solid fractal model of soil density scaling. European Journal of Soil Science 54, 467–476.

Bird, N.R.A., Bartoli, F., Dexter, A.R., 1996. Water retention models for fractal soil structures. European Journal of Soil Science 47, 1–6.

Crawford, J.W., Matsui, N., 1996. Heterogeneity of the pore and solid volume of soil: distinguishing a fractal space from its non-fractal complement. Geoderma 73, 183–195.

Crawford, J.W., Sleeman, B.D., Young, I.M., 1993. On the relation between number size distributions and the fractal dimension of aggregates. Journal of Soil Science 44, 555–565.

Dathe, A., Baveye, P., 2003. Dependence of the surface fractal dimension of soil pores on image resolution and magnification. European Journal of Soil Science 54, 453–466.

Dathe, A., Eins, S., Niemeyer, J., Gerold, G., 2001. The surface fractal dimension of the soil–pore interface as measured by image analysis. Geoderma 103, 203–229.

Dutta, T., Tarafdar, S., 2003. Fractal pore structure of sedimentary rocks: simulation by ballistic deposition. Journal of Geophysical Research, (Solid Earth) 108.

Eins, S., 1998. Special approaches of image analysis for the measurement of fractal dimension. In: Losa, G.A., Merlini, D., Nonnenmacher, T.F., Weibel, E.R. (Eds.), Fractals in Biology and Medicine, vol. II. Birkhäuser, Basel, pp. 86–96.

Gimenez, D., Allmaras, R.R., Nater, E.A., Huggins, D.R., 1997. Fractal dimensions for volume and surface of interaggregate pores—scale effects. Geoderma 77, 19–38.

Gimenez, D., Allmaras, R.R., Huggins, D.R., Nater, E.A., 1998. Mass, surface, and fragmentation fractal dimensions of soil fragments produced by tillage. Geoderma 86, 261–278.

Lehmann, P., Stahli, M., Papritz, A., Gygi, A., Fluhler, H., 2003. A fractal approach to model soil structure and to calculate thermal conductivity of soils. Transport in Porous Media 52, 313–332.

Mandelbrot, B.B., 1983. The Fractal Geometry of Nature. W.H. Freeman and Co., New York.

Niemeyer, J., Machulla, G., 1999. Description of soil pore systems accessible for water by fractal dimensions. Physica. A, Statistical Mechanics and its Applications 266, 203–208.

Pachepsky, Y., Yakovchenko, V., Rabenhorst, M.C., Pooley, C., Sikora, L.J., 1996. Fractal parameters of pore surfaces as derived from micromorphological data: effect of long-term management practices. Geoderma 74, 305–319.

Perfect, E., Kay, B.D., Rasiah, V., 1993. Multifractal model for soil aggregate fragmentation. Soil Science Society of America Journal 57, 896–900.

Perfect, E., McLaughlin, N.B., Kay, B.D., Topp, G.C., 1996. An improved fractal equation for the soil water retention curve. Water Resources Research 32, 281–287.

Perrier, E., Bird, N., Rieu, M., 1999. Generalizing the fractal model of soil structure: the pore-solid fractal approach. Geoderma 88, 137–164.

Rappoldt, C., Crawford, J.W., 1999. The distribution of anoxic volume in a fractal model of soil. Geoderma 88, 329–347.

Reeve, R., 1992. A warning about standard errors when estimating the fractal dimension. Computers and Geosciences 18, 89–91.

Rieu, M., Sposito, G., 1991. Fractal fragmentation, soil porosity, and soil-water properties: 1. Theory. Soil Science Society of America Journal 55, 1231–1238.

Sukop, M.C., Perfect, E., Bird, N.R.A., 2001. Water retention of prefractal porous media generated with the homogeneous and heterogeneous algorithms. Water Resources Research 37, 2631–2636.

Turcotte, D.L., 1986. Fractals and fragmentation. Journal of Geophysical Research, (Solid Earth and Planets) 91, 1921–1926.

Tyler, S.W., Wheatcraft, S.W., 1990. Fractal processes in soil-water retention. Water Resources Research 26, 1047–1054.

Vogel, H.J., 2000. A numerical experiment on pore size, pore connectivity, water retention, permeability, and solute transport using network models. European Journal of Soil Science 51, 99–105.

Young, I.M., Crawford, J.W., 1991. The fractal structure of soil aggregates—its measurement and interpretation. Journal of Soil Science 42, 187–192.